The Astrophysical Journal, 878:6 (12pp), 2019 June 10 https://doi.org/10.3847/1538-4357/ab1b2a


# A Numerical Study of Cosmic Proton Modulation Using AMS-02 Observations

Xi Luo[1,2,3], Marius S. Potgieter[4], Veronica Bindi[3], Ming Zhang[5], and Xueshang Feng[1,2]
[1] SIGMA Weather Group, State Key Laboratory of Space Weather, National Space Science Center, Chinese Academy of Sciences, Beijing 100190, People's Republic of China
[2] School of Astronomy and Space Science, University of Chinese Academy of Sciences, Beijing, 100049, People's Republic of China
[3] Physics and Astronomy Department, University of Hawaii, Honolulu, HI 96822, USA
[4] Center for Space Research, North-West University, Potchefstroom 2520, South Africa
[5] Department of Physics and Space Sciences, Florida Institute of Technology, Melbourne, FL 32901, USA
*Received 2018 September 20; revised 2019 April 6; accepted 2019 April 18; published 2019 June 6*

## Abstract

Since 2011 May, the Alpha Magnetic Spectrometer (AMS-02) on board the *International Space Station* has provided monthly cosmic proton fluxes for various low-rigidity levels ($P < 50$ GV). These precise measurements, in terms of high time and rigidity resolution, have provided a good opportunity to study cosmic ray modulation over a wide range of rigidities, together with transient events. Subsequently, a comprehensive numerical transport model has been constructed, based on Parker's transport equation that includes all known physical mechanisms: diffusion, convection, drift, and adiabatic cooling. Propagating diffusion barriers to simulate Forbush decreases (Fds) and global merged interaction regions (GMIRs) have also been incorporated: (1) utilizing a time-varying tilt angle of the heliospheric current sheet and interplanetary magnetic field, the general trend of the time variation of cosmic proton fluxes has been reproduced; (2) the Fd events in 2011 October and 2012 March have been simulated, and the first GMIR event in solar cycle 24 has also been simulated and studied; and (3) the rigidity dependence of the proton fluxes, as revealed by the AMS-02 data, has been reproduced with the appropriate chosen rigidity dependent diffusion coefficients. In order to reproduce the proton observations, we find that apart from the transient events, the derived mean free paths in interplanetary space also need to be changed with time.

*Key words:* cosmic rays – diffusion – Sun: activity – Sun: heliosphere

## 1. Introduction

Cosmic rays (CRs) are energetic, charged particles that were discovered by Victor Hess in the 1910s. As these particles propagate into the heliosphere, they encounter the outward moving solar wind plasma. Subsequently, the CR intensity is anticorrelated with solar activity and this process is called solar modulation. As irregularities exist in the interplanetary magnetic field (IMF; Parker 1965), which is embedded in the solar wind plasma, this process exhibits the characteristics of particle diffusion. It was later found that the drift motion, which is caused by gradients and curvatures in the IMF, also plays a significant role in the transport process (Jokipii et al. 1977; Kóta & Jokipii 1983; Potgieter & Moraal 1985; le Roux & Potgieter 1995). After introducing a wavy heliospheric current sheet (HCS), its time variations were investigated and it was demonstrated that the HCS tilt angle is a crucial modulation parameter in reproducing the CR 22 yr modulation cycle (Jokipii & Thomas 1981; Potgieter & Moraal 1985; le Roux & Potgieter 1991; Potgieter 2013).

Apart from the drift motion, merged interaction regions (MIRs) are another important concept needed to understand the time-dependent solar modulation process, especially during solar maximum ascending phase periods (Burlaga et al. 1993; Potgieter & le Roux 1994). With a process called "entrainment," the distinct small interaction regions, shocks, and ejecta create larger plasma flow systems called MIRs (Burlaga et al. 1983, 1984). Utilizing the CR and plasma data from the two *Voyager* spacecraft, Burlaga et al. (1985) found that the CR intensity is decreased within these MIRs and the magnetic field is turbulent inside them. Based on *Pioneer* and *Voyager* spacecraft data in solar cycle 21/22, McDonald et al. (1993) concluded that time-dependent solar modulation is mainly caused by global merged interaction regions (GMIRs) and drift effects. Burlaga et al. (1985) analyzed the IMF spectra inside GMIRs, and argued that their modulation effect is related to the scattering of CRs by the embedded turbulence. Consequently, an MIR is usually modeled as a propagating diffusion barrier, in which the diffusion coefficients are reduced (Perko & Fisk 1983; Potgieter et al. 1993; Potgieter & le Roux 1994; le Roux & Potgieter 1995; Luo et al. 2011). Based on the diffusion barrier model, Perko & Fisk (1983) reproduced the CR intensity time variation in solar cycle 21, while Potgieter et al. (1993) numerically modeled GMIR events for solar cycle 22, also including drifts. Additionally, propagating diffusion barriers are also used to simulate smaller CR transient events such as Fd's (le Roux & Potgieter 1991; Luo et al. 2017).

It is worthwhile mentioning that because of recent demands for human space exploration, there is an additional need to fully understand the CR induced space radiation environment (Schwadron et al. 2017) in a time-dependent manner as it changes with solar activity. Because CR flux levels vary with solar activity and heliospheric spatial distance, one of the major challenges is to comprehend this phenomenon physically and then to compose reliable methods for predicting it (Miyake et al. 2017).

Being operational since 2011 May, the Alpha Magnetic Spectrometer 02 (AMS-02) has provided highly accurate CR flux data for a wide range of energies (from 400 MeV/n to a few TeV/n; Bindi et al. 2017). The low-energy part of these spectra provides a unique opportunity to study time-dependent solar modulation during solar cycle 24 (Aguilar et al. 2018a).

As an initial trial, based on a numerical modulation model that also incorporates the diffusion barrier approach for simulating Fd and GMIRs, we investigate the AMS-02 monthly averaged proton spectra from 2011.4 (2011 May) to

2012.89 (2012 November) to come to a better understanding of how solar modulation has changed during this period. To our knowledge, this is the first time the GMIR concept has been adapted for reproducing CR time variations in solar cycle 24.

We present the numerical model and AMS-02 observed proton spectra in Section 2. Specifically, we describe the CR transport equation and stochastic differential equation (SDE) numerical method, as well as the IMF and HCS drift models. Additionally, the diffusion coefficients' analytical expressions and diffusion barrier model are outlined in this section. Next, the AMS-02 monthly proton spectra and our choice of the proton local interstellar spectrum (LIS) are given. In Section 3, the simulation results in comparison with AMS-02 observed spectra are demonstrated. By introducing the Fd and GMIR diffusion barrier approach, together with changing the IMF magnitude, HCS tilt angle, and diffusion coefficients, our numerical results capture the time history for the monthly proton spectra as observed by AMS-02 for the mentioned period. Lastly, a brief summary and outlook are given in Section 4.

## 2. Modulation Model and AMS-02 Proton Spectra

In this section, the numerical model to reproduce the AMS-02 measured spectra for the mentioned period is discussed in detail.

### 2.1. CR Transport and SDEs

The modulation model is based on the transport equation developed by Parker (1965):

$$\frac{\partial f}{\partial t} = -(\boldsymbol{V}_{\rm sw} + \langle \boldsymbol{v}_D \rangle) \cdot \nabla f + \nabla \cdot (K^{(s)} \cdot \nabla f) + \frac{1}{3}(\nabla \cdot \boldsymbol{V}_{\rm sw}) \frac{\partial f}{\partial \ln p}\,, \quad (1)$$

where $f$ is the CR distribution function in the phase space $(\boldsymbol{r}, p)$. The CR flux $j$ measured by experiments is related to the distribution function by $j \propto p^2 f$. Here, $p$ denotes momentum. In experimental studies, particle rigidity $P$ is widely used. It is related to momentum by $P = pc/q$, where $c$ is the speed of light and $q$ is the charge of the CR particles. For protons, the units GeV$/c$ for momentum, and GV for rigidity, are used. $\boldsymbol{V}_{\rm sw}$ is the solar wind speed. It is noted that, in reality, the solar wind speed varies with radial distance and with time, see, e.g., Richardson et al. (2008), Zank et al. (2018), and Zhao et al. (2018). From our previous studies, we know that this modest radial dependence up to the termination shock has an insignificant effect on CR modulation near the Earth; see, e.g., Luo et al. (2013, 2017). Concerning time-dependence, the averaged solar wind speed displays a modest variation over a solar cycle so that its direct impact (through the convection term) on CR modulation is relatively small, but still of fundamental importance, see, e.g., Wibberenz et al. (1998) and Potgieter (2013). Therefore, to focus on CR transient events and their relation to the mean free path (MFP) time variations, the solar wind speed is assumed not to vary with time in our present numerical model.

The solar wind profile inside the termination shock is given by a simplified latitude-dependent model. It is defined by:

$$V_{\rm sw}(\theta) = \begin{cases} 650 \ \ {\rm km\ s^{-1}} \ \text{if} \ \ \theta < \frac{2\pi}{9},\ \theta > \frac{7\pi}{9} \\ 430 \ \ {\rm km\ s^{-1}} \ \text{if} \ \ \frac{2\pi}{9} \leqslant \theta \leqslant \frac{7\pi}{9} \end{cases}, \quad (2)$$

where $\theta$ is the polar angle. The solar wind plasma in the heliosheath is assumed to be incompressible, i.e.,$\nabla \cdot \boldsymbol{V}_{\rm sw} = 0$. Thus, the plasma speed decreases with radial distance $r$ according to the following function:

$$V_{\rm sw} = V(r_{\rm ts})_{\rm sw} \left(\frac{r_{\rm ts}}{r}\right)^2 \ {\rm km\ s^{-1}}, \quad (3)$$

where $V(r_{\rm ts})_{\rm sw}$ is the solar wind speed at the termination shock, which is simplified as a sphere with radial position ($r_{\rm ts}$) 92 au from the Sun.

Under the weak scattering limit (Forman et al. 1974; Ngobeni & Potgieter 2015), the pitch-angle averaged drift velocity is given by:

$$\langle \boldsymbol{v}_D \rangle = \nabla \times \kappa_T \hat{\boldsymbol{e}_B} = \frac{pv}{3q} \nabla \times \left(\frac{\boldsymbol{B}}{B^2}\right). \quad (4)$$

Based on *Ulysses* CR observations (Heber & Potgieter 2006), it was found that the drift coefficient should be reduced at low rigidity with respect to the weak scattering limit expression; also see Potgieter (2013) for a review. The drift velocity is then given by:

$$\langle \boldsymbol{v}_D \rangle_A = \langle \boldsymbol{v}_D \rangle \left(\frac{(p/p_{A0})^2}{1 + (p/p_{A0})^2}\right). \quad (5)$$

The parameter $p_{A0} = 1$ GeV$/c$. In Equation (1), $K^{(s)}$ denotes the diffusion tensor, which has the following form:

$$K^{(s)} = \begin{pmatrix} \kappa_{\parallel} & 0 & 0 \\ 0 & \kappa_{\perp\theta} & 0 \\ 0 & 0 & \kappa_{\perp r} \end{pmatrix}, \quad (6)$$

in the local IMF coordinate system. Here, $\kappa_{\parallel}$ is the parallel diffusion coefficient, while $\kappa_{\perp\theta}$ and $\kappa_{\perp r}$ are the two perpendicular diffusion coefficients in the radial and latitudinal directions, respectively. The MFP, $\lambda$, relates to the relevant diffusion coefficient $\kappa$ by $\lambda = 3\kappa\ /v$, with $v$ as the charged particle's speed.

This equation constitutes the four essential physical processes for the transport of CR in the heliosphere: the solar wind convective term ($-\boldsymbol{V}_{\rm sw} \cdot \nabla f$ ) due to the outward moving solar wind plasma; the drift term ($-\langle \boldsymbol{v}_D \rangle \cdot \nabla f$) due to gradient and curvature drift in the IMF; the diffusive term ($\nabla \cdot (K^{(s)} \cdot \nabla f)$) due to IMF irregularities; and the adiabatic energy loss term $\left(\frac{1}{3}(\nabla \cdot \boldsymbol{V}_{\rm sw}) \frac{\partial f}{\partial \ln p}\right)$ due to the divergence of the solar wind plasma. Our numerical model contains all these processes.

Equation (1) is equivalent to the following two SDEs:

$$d\boldsymbol{X} = (\nabla \cdot K^{(s)} - \boldsymbol{V}_{\rm sw} - \langle \boldsymbol{v}_D \rangle) ds + \sum_{\sigma=1}^{3} \boldsymbol{\alpha}_\sigma d\boldsymbol{W}_\sigma(s)\,,$$
$$dp = \tfrac{1}{3} p (\nabla \cdot \boldsymbol{V}_{\rm sw}) ds\,. \quad (7)$$

Here, $d\boldsymbol{W}_\sigma(s)$ is the Wiener process, which can be numerically generated by the Gaussian random number. $\boldsymbol{\alpha}_\sigma$

can be calculated from the CR diffusion coefficients. In our time-backward numerical simulation, a stochastic process is generated by integrating these two SDEs, which describe the trajectories of the pseudoparticles (or phase space density element). Since Zhang (1999) systematically developed the SDE method to solve the CR transport equation, this approach has been widely used for studying CR solar modulation numerically, see, e.g., Pei et al. (2010), Luo et al. (2011), Kopp et al. (2012), Guo & Florinski (2014), Zhao et al. (2014), Bobik et al. (2016), and Qin & Shen (2017).

Based on the Ito formula, Zhang (1999) demonstrated that the solution to the CR transport equation is:

$$f(t, Q) = \langle f_b(t - \chi, Q_\chi)\rangle. \tag{8}$$

$Q$ is the stochastic process based on the corresponding SDE, and it has the first exit time $\chi$ and exit boundary value $f_b(t - \chi, Q_\chi)$. As the time $t$ is an intrinsic variable in the SDE numerical method, time-dependent problems (transient events) are automatically handled without introducing additional dimensions (Luo et al. 2017, 2018). In our model, the LIS is a steady-state boundary condition, which is a function of energy (or momentum). Equation (8) can be simplified to be $f(t, \boldsymbol{r}, p) = \sum_i f_b^i(p_i)/N$, where $N$ ($N \gg 1$) is the number of the stochastic processes. The SDE method for our CR modulation model is time-backward, thus the time $t$ is iterated as $t_{n+1} = t_n - dt$. By setting the relationship between the diffusion barrier's location and time, $r = f(t)$, the barrier's location $r_n$ can be updated for each iteration step $t_n$. Correspondingly, reduced diffusion and drift coefficients can be calculated (see Equation (15) and its description). Subsequently, the SDE can be integrated to trace the pseudoparticles' trajectory. This is the numerical procedure followed to simulate time-dependent phenomena such as Fds and GMIRs.

### 2.2. IMF and Current Sheet Model

In the numerical model, Parker's IMF model (Parker 1958) is utilized as the background heliospheric magnetic field. The HCS sectors are also included, with the following analytical relationship:

$$\boldsymbol{B}(r, \theta) = \frac{A}{r^2}\left(\hat{e_r} - \frac{r\Omega \sin\theta}{V_{\rm sw}}\hat{e_\phi}\right)[1 - 2H(\theta - \theta_{cs})]. \tag{9}$$

In Equation (9), $r$ and $\theta$ indicate the radial distance and polar angle, respectively; $\Omega$ is the solar rotation angular speed; the constant $A$ is related to the IMF magnitude and direction (sign) near the Earth ($r = 1$ au, $\theta = \pi/2$). $H(\theta - \theta_{cs})$ is the Heaviside function and $\theta_{cs}$ is the polar angle for the HCS surface. The HCS is modeled according to the following analytical expression (Kóta & Jokipii 1983):

$$\cot(\theta_{cs}) = -\tan(\alpha)\sin(\phi^*), \tag{10}$$

where $\phi^* = \phi + \frac{r\Omega}{V_{\rm sw}} - \Omega t$; $\alpha$ is the HCS tilt angle; $\phi$ is the longitude angle for the current sheet surface, while $\phi^*$ is the foot point at the Sun for the corresponding spiral magnetic field line.

Since the magnetic field direction changes abruptly near the HCS, based on Equation (4), the drift velocity due to the Parker IMF model has singularity. The magnitude of this current sheet drift velocity can be expressed as (Jokipii et al. 1977; Burger & Potgieter 1989)

$$|\langle \boldsymbol{v}_{Dcs}\rangle| = \frac{2R_g v}{3r}\delta(\theta - \theta_{cs}), \tag{11}$$

where $R_g$ is the CR particle's gyroradius. It is known that the current sheet drift occurs when a CR particle's distance to the HCS is within $2R_g$ (Burger & Potgieter 1989). This distance can also be expressed as $r\epsilon = 2R_g$, where $\epsilon$ is a small polar angle increment. Because of the following relationship

$$\int_{\theta_{cs}-\epsilon}^{\theta_{cs}+\epsilon} \delta(\theta - \theta_{cs})d\theta = 1 = \int_{\theta_{cs}-\epsilon}^{\theta_{cs}+\epsilon} \frac{r}{4R_g}d\theta, \tag{12}$$

the $\delta$ function appearing in the current sheet drift velocity is approximated by $r/4R_g$ within the range of $(\theta_{cs} - \epsilon, \theta_{cs} + \epsilon)$. Correspondingly, the magnitude of $|\langle \boldsymbol{v}_{Dcs}\rangle|$ is approximated as $v/6$. Because the current sheet drift velocity is along the local HCS surface and perpendicular to the magnetic field, the following expression can be constructed:

$$\langle \boldsymbol{v}_{Dcs}\rangle = \frac{v}{6}(\sin\Psi\cos\zeta\hat{e}_r + \sin\zeta\hat{e}_\theta + \cos\Psi\cos\zeta\hat{e}_\phi). \tag{13}$$

Here, the angle $\zeta$ is the angle between the local HCS surface's normal direction $\hat{n}$ and the $-\hat{e_\theta}$ direction, and $\Psi$ is the IMF spiral angle. The HCS is assumed to be locally flat, thus the distance to the HCS from the nearby location $(r, \theta, \phi)$ is approximated as $d = |r(\theta - \theta_{cs})\cos\zeta|$. Additionally, to avoid the situation of the pseudoparticle's direct crossing of the HCS, a forth-order Runge–Kutta method is implemented to treat the HCS drift in our SDE numerical model. See Luo et al. (2017, 2018) for additional detail on our HCS drift model.

As the solar wind plasma propagates outward in the heliosphere and changes with solar activity, the outward propagating modulation conditions that affect CRs usually span over one year (Potgieter et al. 2014, 2015). The CR flux at Earth is always lagging behind in response to solar activity variations; see le Roux & Potgieter (1992). Therefore, in our numerical model, 13 month averaged interplanetary parameters are utilized (tilt angle and IMF magnitude at 1 au) to simulate the AMS-02 proton spectra. Figure 1 illustrates the monthly averaged IMF magnitude at the Earth[6] and the HCS tilt angle.[7] The 13 month averaged values, which reflect the changing interplanetary conditions in the numerical model, are shown in both panels.

### 2.3. Diffusion Coefficients and Diffusion Barrier Model

When CR particles propagate inward from the outer heliosphere, they encounter the IMF irregularities, which scatter the CR particles, providing the diffusion nature of their transport. There are two perpendicular and one parallel diffusion coefficients, as Equation (6) displays. With perpendicular diffusion, CR particles can cross the mean spiral IMF lines to reach the Earth eventually. Over the last decades, significant progress in understanding the diffusion process based on turbulence theory has been made; see for example Jokipii (1966), Bieber et al. (1994), Zank et al. (1998), Qin et al. (2002), Teufel & Schlickeiser (2002), Chhiber et al. (2017), and Zhao et al. (2017, 2018). Recently, based on an incompressible magnetohydrodynamics formulating 2D slab

[6] Data from http://www.srl.caltech.edu/ACE/ASC/index.html.
[7] Data from http://wso.stanford.edu/; the "classic" HCS model is used.

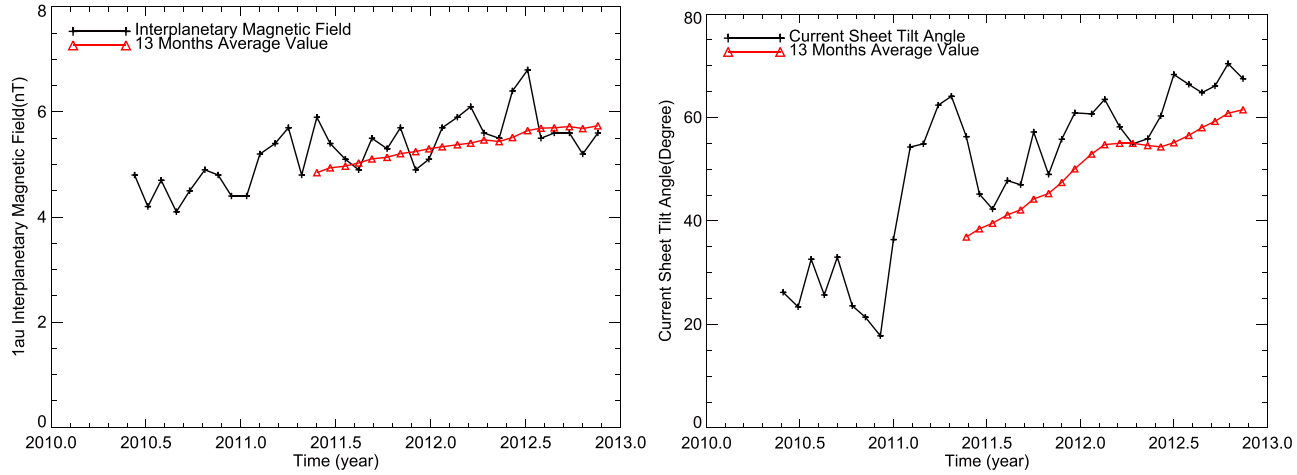


**Figure 1.** Left: monthly averaged IMF values measured by the *ACE* satellite from 2010 to 2013. Right: HCS tilt angle for the same period. The 13 month averaged values from 2011.4 to 2012.89 are plotted as red triangles.

turbulence transport model (Zank et al. 2017), Zhao et al. (2017) calculated the parallel and perpendicular MFPs from the quasilinear theory and nonlinear guiding center theory. It predicts the rigidity dependence for the parallel MFP, namely $\lambda_{\parallel} \propto P^{0.33}$ over the rigidity range [10MV, $10^3$MV], with the slope steepening as $P > 10^3$ MV for nearly all radial distances. As the calculation is confined within the supersonic solar wind region (<75 au), the situation is still unknown for the region near the termination shock and inside the heliosheath. Based on a similar turbulence approach, Zhao et al. (2018) demonstrated that the MFPs $\lambda_{\parallel}$, $\lambda_{\perp}$, and $\lambda_{rr}$ almost do not change with solar activity, if the background IMF changes in concert with the turbulence levels in response to solar activity. Such unchanging MFPs cannot reproduce the CR solar cycle variations (11 yr cycles). It follows that there are still obstacles to overcome for directly adapting and applying the turbulence based approach to CR modulation modeling. The present study is focused on using an SDE numerical approach together with a diffusion barrier model to reproduce the time-varying AMS-02 proton spectrum. Therefore, a phenomenological functional form (Equation (14)) for the diffusion coefficients is chosen to fulfill this task. This particular approach has already been used to reproduce PAMELA proton spectra (Potgieter et al. 2014) and electron spectra (Potgieter et al. 2015; Di Felice et al. 2017) from 2006 to 2009. Luo et al. (2018) also adapted this functional form to simulate electron Fds for the first time; see also Munini et al. (2018). In this context, we prefer to simplify rather than complicate our modeling approach using SDEs, which is inherently complicated and rather tedious, especially when comparisons are made to observations.

The diffusion coefficients are expressed as a function of the local IMF magnitude and particle rigidity:

$$\kappa_{\parallel} = \kappa_{\parallel 0}\beta\frac{B_0}{B}\left(\frac{P}{P_k}\right)^{a_{\parallel}}\left[1+\left(\frac{P}{P_k}\right)^{\frac{b_{\parallel}-a_{\parallel}}{c_{\parallel}}}\right]^{c_{\parallel}}$$
$$\kappa_{\perp_r,\perp_\theta} = (\kappa_{\perp_r 0,\perp_\theta 0})\beta\frac{B_0}{B}\left(\frac{P}{P_k}\right)^{a_{\perp}}\left[1+\left(\frac{P}{P_k}\right)^{\frac{b_{\perp}-a_{\perp}}{c_{\perp}}}\right]^{c_{\perp}}. \quad (14)$$

In these equations, $B$ is the magnitude of the local IMF with $B_0 = 1$ nT. $P$ is the rigidity in GV, and $\beta$ is the ratio between particle speed and the speed of light. The rigidity dependence of these diffusion coefficients evidently consists of two power laws. This double power-law shape may become inconspicuous for some parameters. In these equations, $\kappa_{\parallel 0}$ and $\kappa_{\perp_r 0,\perp_\theta 0}$ have the unit of $10^{20}$ cm$^2$ s$^{-1}$; $P_k$, $a_{\parallel}$, $b_{\parallel}$, $c_{\parallel}$, $a_{\perp}$, $b_{\perp}$, $c_{\perp}$ are parameters that define the rigidity dependence of the diffusion coefficients over the range of interest to solar modulation studies. They are adjusted until the simulated monthly spectra reproduce the corresponding AMS-02 proton spectra. To simulate a GMIR, a three-dimensional (3D) propagating diffusion barrier is incorporated in the model, defined by the following analytical function (Luo et al. 2011, 2017, 2018):

$$\kappa'_{\parallel,\perp,T} = \frac{\kappa_{\parallel,\perp,T}}{[1+\rho h(\theta)f(r)g(\phi)]}. \quad (15)$$

Here, $\kappa'_{\parallel,\perp}$ represents the diffusion coefficients inside the diffusion barrier; $\kappa'_T$ is the drift coefficient inside the diffusion barrier; $\rho$ is a constant determining the reduction level of the diffusion and drift coefficients inside the barrier; $h(\theta)$ determines the diffusion barrier's latitudinal profile, which is prescribed by the extent parameter $\theta_{\rm br}$. Its longitudinal profile is defined by the function $g(\phi)$ using the extent parameter of $\phi_{\rm br}$.

$$h(\theta) = e^{-\left(\frac{\theta-\pi/2}{\theta_{\rm br}}\right)^{10}},$$
$$g(\phi) = e^{-\left(\frac{\phi}{\phi_{\rm br}}\right)^{10}}. \quad (16)$$

The radial profile is defined by $f(r)$, given by:

$$f(r) = \begin{cases} 1-\frac{r-r_{\rm cen}}{r_a} & \text{if } r_{\rm cen} < r < r_{\rm sh} \\ \frac{r-r_{\rm end}}{r_b} & \text{if } r_{\rm end} < r \leqslant r_{\rm cen} \\ 0 & \text{if } r \leqslant r_{\rm end},\ r \geqq r_{\rm sh}. \end{cases} \quad (17)$$

The diffusion barrier has a leading part with a width of $r_a$ and a trailing part of width $r_b$. See Luo et al. (2017) for more details.

Following *Voyager* observations (Burlaga et al. 2003) and our previous numerical work about GMIRs (Luo et al. 2011), the radial width of the GMIR barrier model is taken as $L = 11.5$ au, specifically with $r_a = 1.5$ au and $r_b = 10$ au. The GMIR barrier has a full longitudinal extent, namely $\phi_{\rm br} = \pi$ with its latitudinal extent $\theta_{\rm br} = \pi/4$.

As a test case of our GMIR model, Figure 2 demonstrates the CR flux variations at 1 au in response to a "single simulated

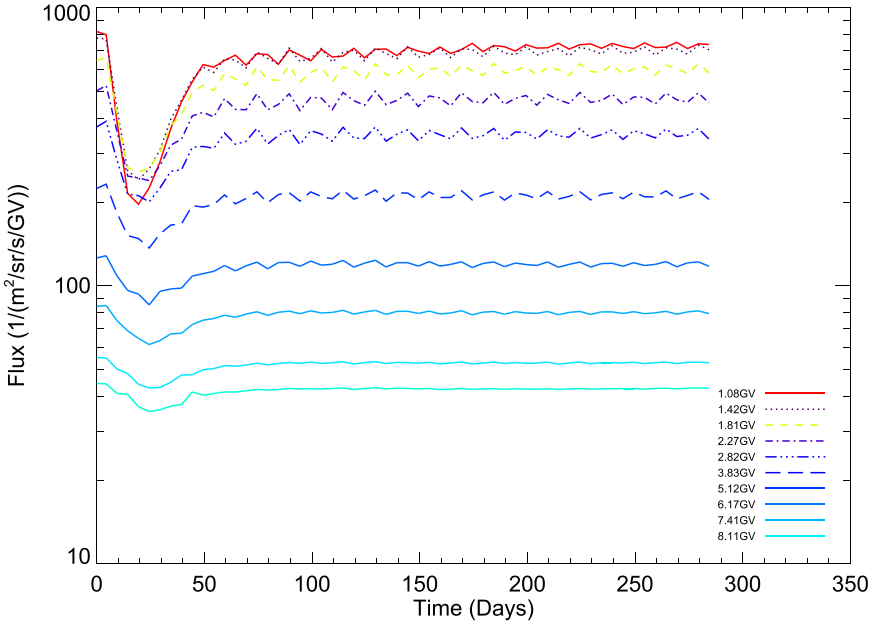


**Figure 2.** Computed proton flux at Earth (1 au) for the indicated range of rigidities as a function of time in response to a single simulated GMIR propagating outward through the heliosphere as described in the text.

GMIR" propagating from the Sun to the outer heliosphere with a speed of $\sim$500 km s$^{-1}$. These simulation results illustrate the general features of the CR intensity caused by a GMIR; the time variation profile of the flux exhibits a sharp decreasing phase followed by a prolonged recovery phase. The recovery phase lasts hundreds of days until the GMIR propagates fully out of the heliosphere. And, it depends on the 3D size of the particular GMIR. As the GMIR arrives at 1 au, the decrease in flux can be as large as 76% for $\sim$1 GV protons. The GMIR effect diminishes as the CR rigidity increases; for $\sim$8 GV protons, the decrease magnitude is about 11%. In reality, a GMIR is usually formed beyond 10 au (Burlaga et al. 1993), so that such a sharp decrease as illustrated in Figure 2 has never been observed. In our simulation, to reflect the effect of a GMIR formed at $R_{\rm gmir}$ ($R_{\rm gmir} \geqslant 10$ au) on the observer's location at 1 au, the simulation should start from the time of $R_{\rm gmir}/V_{\rm gmir}$ ($V_{\rm gmir}$ is the GMIR propagation speed), which has already been in its recovery phase.

Following Luo et al. (2017, 2018), simulating a much smaller Fd event, the barrier's width is reduced to $L = 0.5$ au, with a limited longitudinal and latitudinal extent, i.e., $\phi_{\rm br} = 2\pi/3$, $\theta_{\rm br} = \pi/4$.

### 2.4. Observed Proton Spectra and the LIS

Large CR detectors launched into geospace measure CR spectra with unprecedented high time resolution; see, e.g., the PAMELA proton observations reported by Adriani et al. (2013), Di Felice et al. (2017), Boezio et al. (2017), Martucci et al. (2018), and Munini et al. (2018). The AMS-02, which was installed on the *International Space Station*, is the largest of these space magnetic spectrometers (Bindi et al. 2017). Starting from 2011 May, it has provided CR spectra ranging from 400 MeV/n up to a few TeV/n. Solar modulation effects have been clearly observed for the lower energy part of these spectra (Aguilar et al. 2018a). We focus on the AMS-02 monthly proton spectra[8] in the rigidity range from 1 to 11 GV (kinetic energy from 0.49 to 10.59 GeV) shown in Figure 3. The dashed lines and triangles depict the monthly averaged proton spectra measured by the AMS-02 experiment. Specifically, 2011.4, 2011.62, 2011.77, 2012.15, 2012.3, 2012.52, 2012.6, and 2012.89 are denoted with different colors. The corresponding LIS is plotted as a black solid line with crosses.

It is shown in the left panel that below 10 GV the CR proton spectra become systematically lower from 2011.4 (2011 May) to 2012.89 (2012 November) in response to solar activity ascending during this period. It should be noted that the monthly spectrum in 2011.77 (2011 October) is lower than that in 2012.15 (2012 February), which is a signature of the occurrence of a transient event (Fd or GMIR effect). In the following section, it will be demonstrated that an Fd event occurred in 2011 October.

It was demonstrated that there is nearly no modulation beyond the heliopause (HP; Luo et al. 2015, 2016; Zhang et al. 2015). When *Voyager 1* crossed the HP in 2012 August (Stone et al. 2013; Webber & McDonald 2015), the spacecraft had begun to measure the very LIS for various CR species (Cummings et al. 2016). These data sets provide the first constraint for the lower energy part of the proton LIS, together with the higher energy part measured by the near Earth detectors, so that a much more reliable LIS can be obtained; see for example Potgieter (2014), Potgieter et al. (2014), Bisschoff & Potgieter (2016), and Herbst et al. (2017). Here, we use the LIS expression from Corti et al. (2016), based on a least-square fit given a well-defined parameterization form. This LIS constitutes the outer boundary condition for the simulation model specified at the HP. Similar to Luo et al. (2017), an absorbing boundary condition is used for the inner boundary.

[8] The measured flux is averaged over one Bartels rotation (Aguilar et al. 2018a).

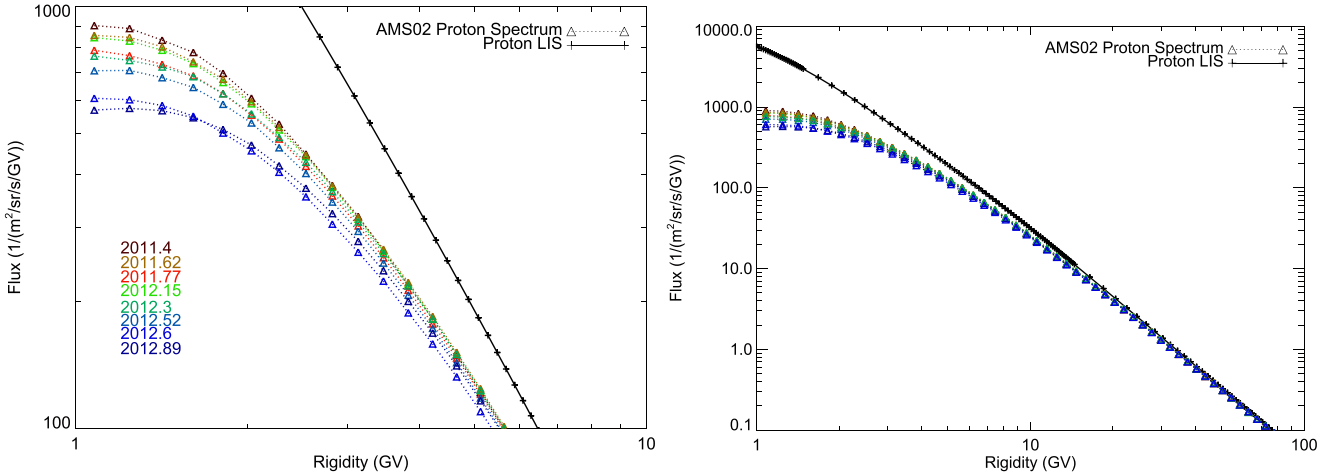


**Figure 3.** Observed monthly averaged proton spectra from the AMS-02 detector for eight different time slots, indicated by triangles and lines of different colors; solid black line with crosses denotes the assumed LIS. Note that the rigidity range differs for the two panels to emphasize what happens at lower and higher values.

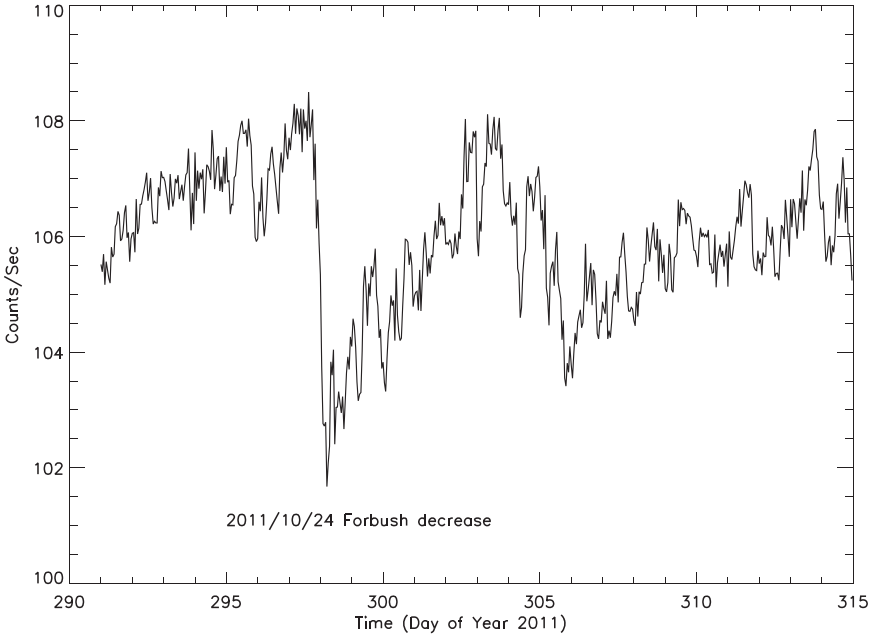


**Figure 4.** Oulu neutron monitor observations from 2011 October 21 to November 10. Evidently, an Fd event was recorded on October 24.

## 3. Results and Discussion

In this section, we present simulated proton spectra at the Earth in comparison with the AMS-02 observations. In addition, the time variation for the MFP's rigidity dependence and the modulation effect of the simulated GMIR event are discussed.

### 3.1. Simulation Strategy

A halo coronal mass ejection (CME) in 2011 October 22 was observed with the Large Angle and Spectrometric Coronagraph on board the *Solar and Heliospheric Observatory* (*SOHO*).[9] Additionally, the ground level neutron monitor in Oulu observed a transient CR decrease in 2011 October 24 (Figure 4). Thus, we argue that an Fd event happened in 2011 October 24, which caused the proton spectrum to become lower. An Fd-model is applied to reproduce this 2011.77 (2011 October) monthly spectrum.

On 2012 March 7 a fast CME occurred (Liu et al. 2013) so that another significant Fd-type event followed on 2012 March 8 (Zhao & Zhang 2016). We attribute the driver for this CR intensity decrease and lower proton spectrum in 2012.22 to this event. Again the Fd-model is applied to simulate these transient effects in the spectra.

Additionally, Liu et al. (2014) reported that a series of CMEs were emitted by the Sun in 2012 March, and demonstrated that they interact with each other and merge into a GMIR eventually. From 2011 to 2013 the global IMF polarity was negative ($A < 0$) and solar activity had increased gradually to approach its maximum for solar cycle 24. As Potgieter & le Roux (1994) stated, GMIRs provide a natural and convincing explanation for the large step decreases in CR modulation, and their occurrence may dominate the modulation process especially during the ascending phase of the solar cycle toward the period of maximum activity. Therefore, similar to the work

[9] https://cdaw.gsfc.nasa.gov/CME_list/UNIVERSAL/2011_10/univ2011_10.html

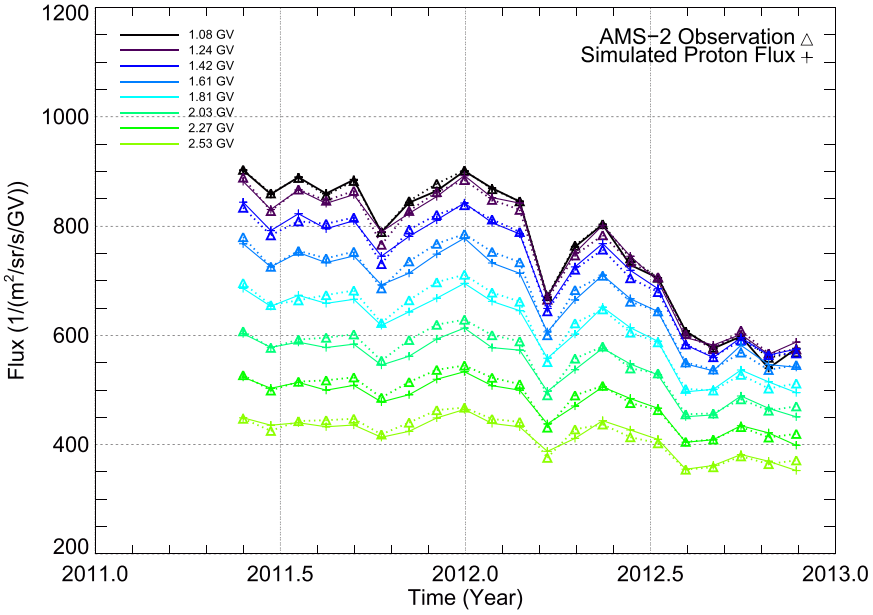


**Figure 5.** Observed AMS-02 proton flux (triangles) for eight different rigidity values, overlaid with the corresponding numerical simulations (plus symbols) from 2011.4 to 2012.89. The rigidity range is from 1.08 to 2.53 GV. Overall, solar activity has been ascending and the flux therefore decreases during this period. The 13 month averaged HCS tilt angle had increased from 36.°9 to 61.°5, and the averaged HMF magnitude at the Earth had changed from 4.8 to 5.7 nT.

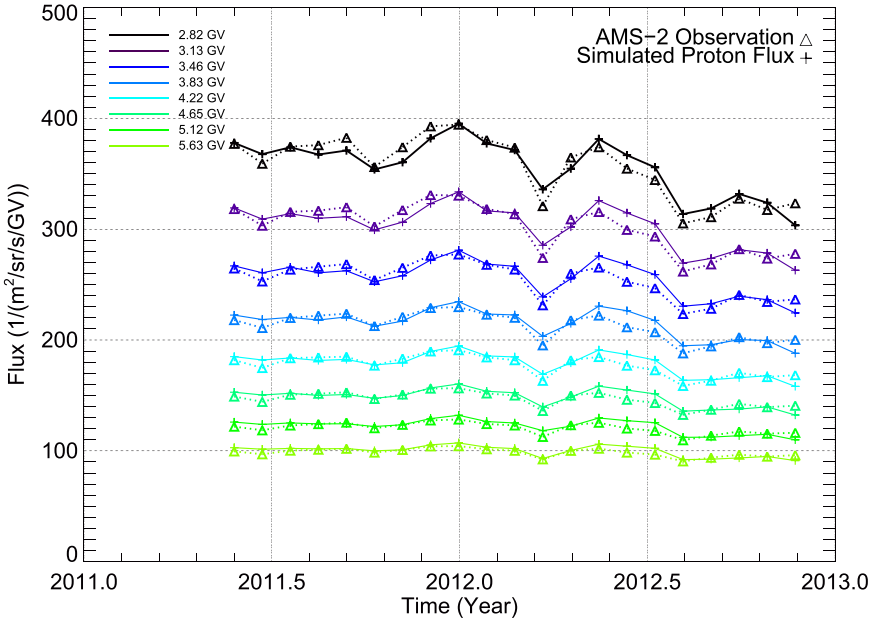


**Figure 6.** Similar to Figures 5, now with a rigidity range from 2.82 to 5.63 GV. Evidently, the modulation effect is less than in the previous figure.

of simulating the CR time variations in solar cycle 21 (Perko & Fisk 1983) and in cycle 22 (Potgieter et al. 1993), it is reasonable to utilize a GMIR to reproduce the CR intensity decrease in solar cycle 24. Subsequently, our GMIR model is applied to reproduce the AMS-02 monthly averaged proton flux in 2012.6 (2012 July) and thereafter. Following Potgieter et al. (1993), the GMIR is assumed to be formed effectively at 15 au, so that to reflect its effect on CRs' observation at 1 au, the simulation time starts from 15 au/500 km $s^{-1}$ $\approx$ 52 days in our time-dependent model.

### 3.2. Simulated Spectra

In Figures 5–7, the simulated proton fluxes are shown in comparison with the corresponding AMS-02 monthly averaged fluxes, from 2011.4 (2011 May) to 2012.89 (2012 November). Note that the flux-unit is $(m^2\ sr\ s\ GV)^{-1}$, which is as such a differential intensity. In Figure 5, the rigidity levels are 1.08, 1.24, 1.42, 1.61, 1.81, 2.03, 2.27, and 2.53 GV, respectively. Similarly, there are eight rigidity levels from 2.82 to 5.83 GV for Figure 6, whereas in Figure 7 the rigidity levels are from 6.17 to 11.49 GV. The AMS-02 monthly proton fluxes are depicted by triangles, while the crosses denote the simulated proton fluxes. From 2011.4 to 2012.89, the Sun's is in an ascending phase as activity is approaching its maximum levels.

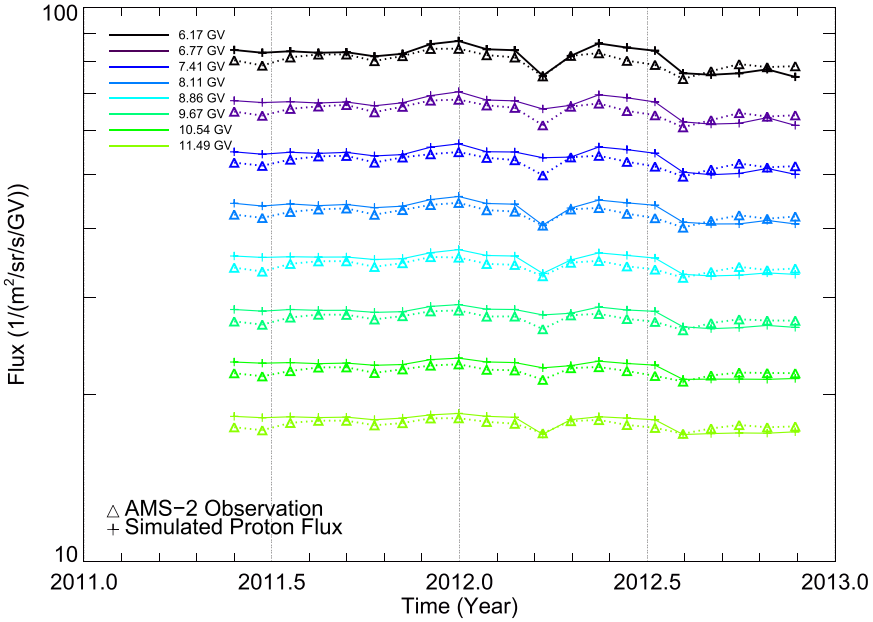


**Figure 7.** Similar to Figures 5 and 6, now for the rigidity range from 6.17 to 11.49 GV. The modulation effect is significantly less than in the previous figures; note the different flux-scale used in the three figures.

Correspondingly, the CR flux value decreases in response to the increasing solar activity. It follows that, as expected, the modulation effect is more significant for lower rigidity particles during the mentioned period. The decrease level is ∼37% for 1.08 GV protons while for 2.53 GV, it only decreases ∼17%. Above about 6 GV, the modulation effect becomes progressively less evident. These results are consistent with PAMELA proton observations reported recently by Martucci et al. (2018); see also Di Felice et al. (2017) and Munini et al. (2018).

As illustrated in Figure 1, both the IMF magnitude and HCS tilt angle, as proxies for solar modulation conditions (Potgieter et al. 2014), increase during this ascending phase. Utilizing these two proxy parameters, our numerical model reproduces the general trend for the proton's time variations.

The monthly averaged AMS-02 proton flux decreased because of the Fd event in 2012.22. This decrease is well reproduced with our diffusion barrier model. A notable feature is that both observations and simulations reveal that the decrease magnitude declines as the proton rigidity increases. Solving the simplified 1D transport equation, Chih & Lee (1986) illustrated that larger diffusion coefficients cause the Fd magnitude to decrease; see le Roux & Potgieter (1991) for a 2D drift scenario. Based on a 3D numerical model, Luo et al. (2017) demonstrated that the Fd magnitude indeed decreases as the CR energy increases. According to our choice for the rigidity dependence of the diffusion coefficients (Equation (14) and Figure 10), the diffusion coefficients increase as the rigidity increases. Correspondingly, in the higher rigidity range we do not see large levels of decrease.

As discussed previously, the CR flux made a step decrease in 2012.6 (2012 July) because of an assumed GMIR event. To study this aspect, a single GMIR diffusion barrier is utilized in the numerical model to simulate the monthly spectra after 2012.6. As it was shown in Figures 5–7, the numerical results reproduce the main features of the CR step decrease for different rigidity levels. Since the GMIR is long-lived and therefore affects the CR transport in the outer heliosphere as well (Potgieter et al. 1993; Burlaga et al. 2003), the following flux variation of several months is actually during the recovery phase of the GMIR event. The CR flux near the Earth has been affected as the GMIR propagates outward.

In order to clarify further the effect on CR transport of the GMIR model, Figure 8 provides a direct comparison between the simulated spectrum with the GMIR (red triangles) and the base simulation without the GMIR (blue asterisks) for 2012.6, 2012.67, 2012.74, and 2012.82. The black plus symbols denote the AMS-02 observations, while the green crosses denote the LIS. The spectrum has been significantly suppressed due to the GMIR, which evidently acts as a CR diffusion barrier. The simulated spectrum with the GMIR agrees satisfactorily with the AMS-02 observations.

According to the proton LIS, the CR flux decreases systematically with increasing rigidity. However, during the GMIR event as shown in Figure 2, the simulated flux for 1.08 GV protons can become lower than that at 1.42 GV and 1.81 GV. In 2012.82, the AMS-02 monthly averaged CR flux at 1.08 GV is 559.2 $(m^2\ sr\ s\ GV)^{-1}$, which is indeed lower than the 1.42 GV flux value of 564 $(m^2\ sr\ s\ GV)^{-1}$. See also the right lower panel of Figure 8. Utilizing the GMIR model, this feature has been naturally reproduced.

Up to this stage, our study has been done in a qualitative manner. As a next step, we shall quantitatively study how the long-term, global decrease is related to rigidity. Such a study can clarify the relationship and even shed light on the rigidity dependence of the three diffusion coefficients, in particular if a bend (kink) in this rigidity dependence is required, or not, as found necessary by Potgieter et al. (2014), to reproduce PAMELA proton spectra from low to high rigidities; see also the review by Potgieter (2017).

### *3.3. Time Variation of MFPs*

The parameters in the expressions for the diffusion coefficients are systematically tuned until the simulated spectra reproduce the corresponding AMS-02 monthly averaged flux. Specifically, the values of these parameters for the Fd and GMIR events are illustrated in Table 1. Figure 9 demonstrates

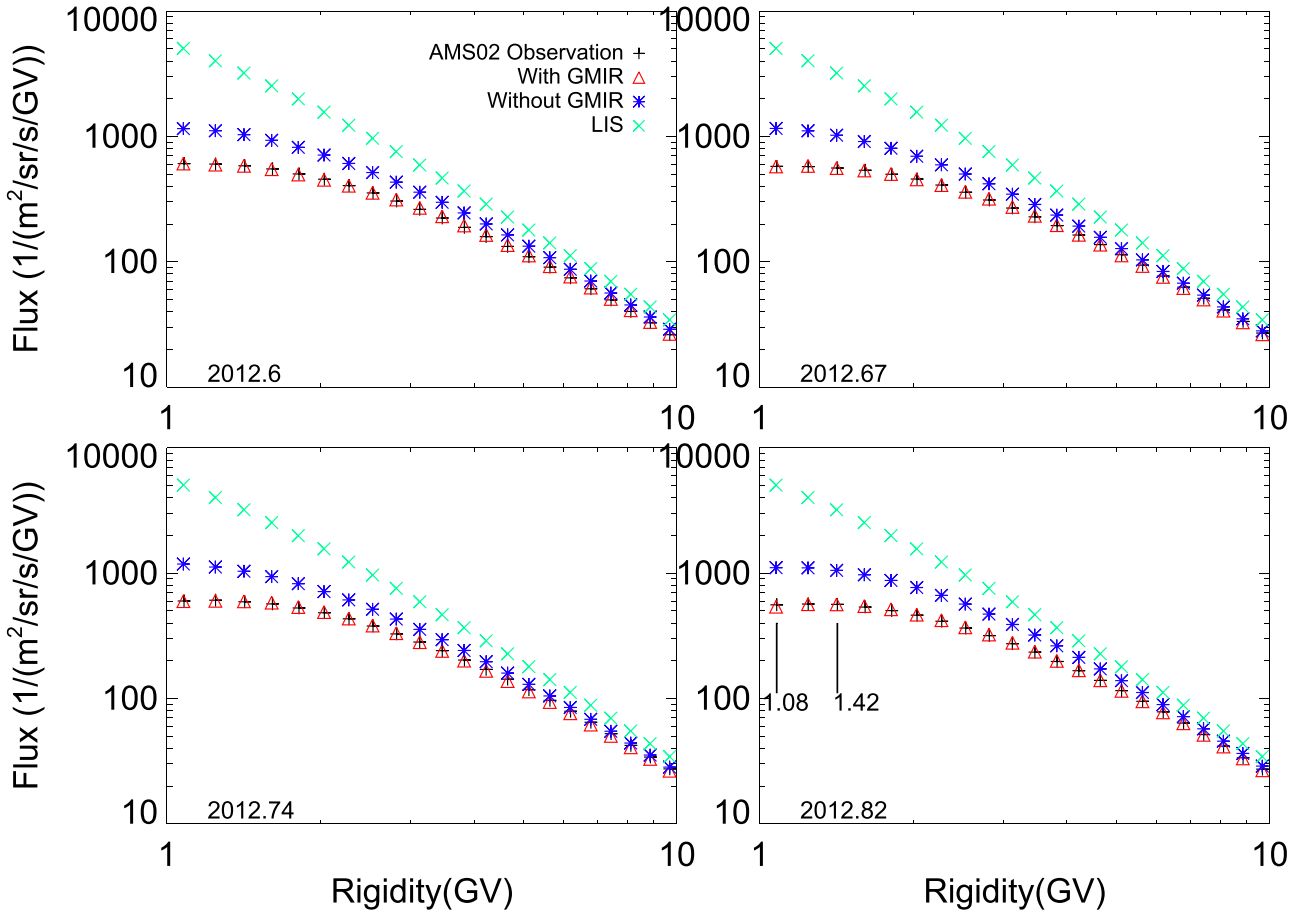


**Figure 8.** Comparison between the simulated spectra for four periods, first with the simulated GMIR (red triangles) and then the base simulation without the GMIR (blue asterisks), all with respect to the proton LIS (green crosses) and in comparison with the corresponding AMS-02 observed proton spectrum (black crosses).

**Table 1**
Values of Different Parameters in the Expressions for the Diffusion Coefficients During the Simulated Fd and GMIR Events, Respectively

| Specific Event and Time | $a_{\parallel}$ | $b_{\parallel}$ | $c_{\parallel}$ | $\kappa_{\parallel 0}$ | $\kappa_{\perp\theta 0}$ | $\kappa_{\perp r0}$ |
|---|---|---|---|---|---|---|
| Fd event 2011.77 (2011 October) | 1.5 | 1.6 | 0.95 | 1300 | 18 | 16 |
| Fd event 2012.22 (2012 March) | 1.3 | 1.5 | 1.0 | 1105 | 22.1 | 13.8 |
| GMIR event 2012.6 (2012 July) | 1.8 | 2.0 | 1.0 | 1615 | 32.3 | 20.1 |
| 2012.67 | 1.5 | 1.7 | 1.0 | 1325 | 26.5 | 16.5 |
| 2012.74 | 1.5 | 1.7 | 1.0 | 1285 | 25.7 | 16.0 |
| 2012.82 | 1.9 | 2.1 | 1.0 | 1365 | 27.3 | 17.0 |
| 2012.89 | 1.8 | 2.0 | 1.0 | 1370 | 27.4 | 17.1 |

**Note.** The parameter $P_k$ is fixed to 4.3 GV for both $\kappa_{\parallel}$ and $\kappa_{\perp}$. Parameters $a_{\perp} = 0.8$, $b_{\perp} = 1.0$, and $c_{\perp} = 2.2$ are also fixed. $a_{\parallel}$, $b_{\parallel}$, $c_{\parallel}$, $a_{\perp}$, $b_{\perp}$, and $c_{\perp}$ are nonunit parameters, while the units for $\kappa_{\parallel 0}$, $\kappa_{\perp\theta 0}$, and $\kappa_{\perp r0}$ are $10^{20}$ cm$^2$ s$^{-1}$.

the radial dependence of the diffusion coefficients ($\theta = \pi/2$, $\phi = 0$) for different time slots. From 2012.6, the GMIR model is incorporated to simulate the AMS-02 spectra. Correspondingly, for the 2012.67 and 2012.89 cases, both $\kappa_{\parallel}$ and $\kappa_{rr}$ are significantly reduced inside the GMIR. Additionally, Figure 9 illustrates that the value of $\kappa_{\parallel}$ decreases from 2011.4 to 2012.89, but there is no clear trend for the time variation of $\kappa_{rr}$.

According to Equation (14), the rigidity dependence of the diffusion coefficients can be obtained after the relevant parameters are constrained by reproducing the observed spectra. The left panel of Figure 10 demonstrates the rigidity dependence of the MFPs ($\lambda = 3\kappa/v$) during specific time periods. It should be noted that due to the constrained parameters, the double power-law shape for Equation (14) become indistinguishable in this plot.

Based on the observations made with the *Advanced Composition Explorer* (*ACE*) near the Earth, Mewaldt et al. (2010) reported that $\lambda_{\parallel}$ had increased as solar activity descended from 2002 to 2009. In order to reproduce the PAMELA spectra, it was shown that both the parallel and perpendicular MFPs for low-rigidity protons needed to be increased from 2006 to 2009 (Potgieter et al. 2014). Similar work was also done by Zhao et al. (2014), who argued that as solar activity was descending from 2006 to 2009, the magnetic field turbulence levels decreased. The lower turbulence level results in a larger parallel MFP ($\lambda_{\parallel}$) and a larger scaling factor for the perpendicular diffusion coefficients ($\lambda_{\perp r}/\lambda_{\perp\theta}$).

Concerning this study, it is expected that $\lambda_{\parallel}$ should decrease during the period 2011.4–2012.89 because solar activity was ascending then. The right panel in Figure 10 illustrates the time variation of the MFPs for 1 GV protons at the Earth from 2011.4 to 2012.89; $\lambda_{\parallel}$ decreases from 1.99 au in 2011.4 to 1.20 au in 2012.89, whereas $\lambda_{\perp r}$ decreases from 0.073 to 0.059 au, and $\lambda_{\perp\theta}$ from 0.045 to 0.037 au. However, the left panel of Figure 10 does not exhibit a clear trend for the time variations of the MFPs. Additionally, their rigidity dependence does not show an explicit bend (kink) at the high rigidity end as used in the work of Potgieter et al. (2014). Illustrated by the left

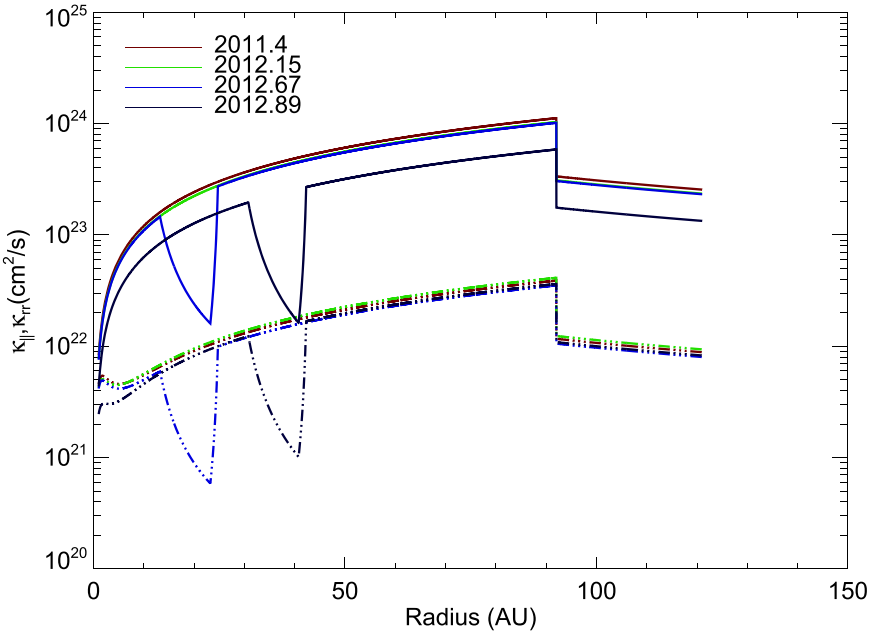


**Figure 9.** Radial dependence of the diffusion coefficients $\kappa_{||}$ and $\kappa_{rr}$ for 1 GV protons for four different representative time slots (2011.4, 2012.15, 2012.67, and 2012.89). The solid line is for $\kappa_{||}$, while the dotted–dashed line illustrates the radial dependence of $\kappa_{rr}$.

panel of Figure 10, the MFPs in the high rigidity end still varies with time. Since our simulation period only spans about 20 months, we cannot draw further conclusions about it. As a next step, we plan to extend our simulation period and use a more robotic or automated statistical fitting method, such as the Markov chain Monte Carlo method (Putze et al. 2009), instead of the current rather tedious manual parameter adjustments.

An interesting feature shown in the right panel of Figure 10 is that the variation of $\lambda_{||}$ exhibits a wave pattern when the diffusion barrier is introduced to the simulation. A recent study by Zhao et al. (2018) also reveals that instead of linearly decreasing or increasing, the MFP variation shows oscillations. It is possible that even if the background diffusion coefficients increase, as long as the diffusion coefficients inside the diffusion barrier are significantly reduced, the net effect of the background and the diffusion barrier still causes the diffusion coefficients (or MFPs) to decrease during this period.

## 4. Summary and Outlook

As the precise measurement of low-energy cosmic proton fluxes by AMS-02 have become available, we have constructed a comprehensive time-dependent modulation model to reproduce the observed monthly spectra from 2011.4 to 2012.89. This numerical transport model, based on the SDE approach, contains all known modulation mechanisms: diffusion, convection, drift, and adiabatic cooling. In addition, combined Fd and GMIR models have been incorporated in the modeling approach. Adapting the observed time-varying IMF magnitude and HCS tilt angle as proxy parameters for solar activity, the detailed trends in the observed proton spectra are reproduced for the mentioned period by additionally adjusting the diffusion coefficients with changing solar activity. Our study is focused on the monthly averaged proton spectral data, as such a high time-resolution study was not possible before, with the exception of the PAMELA observations.

The AMS-02 monthly proton spectra have confirmed that CR modulation is highly rigidity dependent, with the low-rigidity protons experiencing significantly more modulation. This rigidity dependence has been investigated and reproduced by our numerical model. In addition, a unique attribute for the numerical model is that diffusion barriers (to simulate Fds or GMIRs) have been incorporated into our original, time-dependent CR transport model. Subsequently, the Fd events in 2011 October and 2012 March are simulated, whereas the GMIR model provides a natural interpretation for the decrease in the proton intensity after 2012 July. This is the first time that a GMIR event has been studied for solar cycle 24, validating that the GMIR concept is required in order to reproduce the observed proton flux variations in solar cycle 24. Supporting previous solar modulation studies using CR protons (Potgieter et al. 2014; Zhao et al. 2014), our investigation discloses the rigidity dependence of the diffusion coefficients and how important this is for simulating the observed modulation spectra for the mentioned period.

We found that the bend (break) in the rigidity dependence of the MFPs required to explain the AMS-02 proton spectra for the period of 2011.4 to 2012.89 is less than what Vos & Potgieter (2016) reported, when comparing their modulation model to the PAMELA proton spectra for the period 2006–2009. This aspect needs to be investigated further given that the period we studied is relatively short. Since the AMS-02 proton spectra are observed very precisely to high rigidities, the now published and future data can be used effectively in this context.

In order to reproduce the AMS-02 spectra in detail it was required that the three MFPs be varied with time during this 20 month period. It was found that for 1 GV protons at the Earth, the MFPs had to decrease during this period. We emphasize that the MFP time-variations, simulated Fd events, as well as a GMIR event combined in a single time-dependent numerical model are needed to reproduce the AMS-02 spectra. It is concluded that only simulating CR transients cannot reproduce the time trends in the observed spectra for the mentioned period.

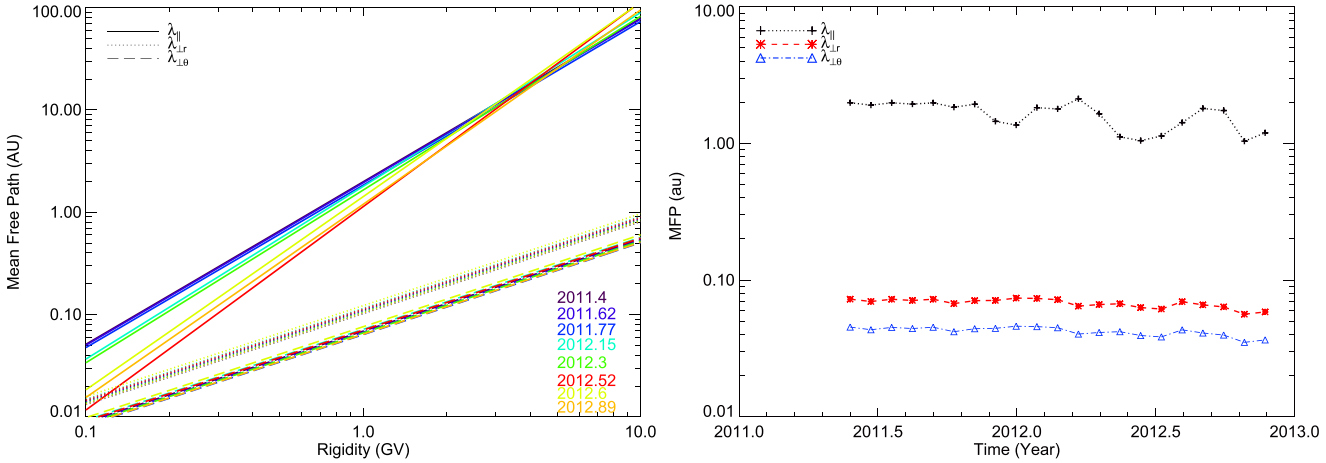


**Figure 10.** Left panel demonstrates the rigidity dependence of the proton MFPs near the Earth. Eight different time slots, 2011.4, 2011.62, 2011.77, 2012.15, 2012.3, 2012.52, 2012.6, and 2012.89, are shown as an illustration of how these MFPs vary with time. They are obtained by reproducing the AMS-02 monthly proton flux shown in Figures 5–7. The right panel illustrates the time variation of the three MFPs for 1 GV protons at the Earth.

In this context, we note that as more precise CR spectra become available, e.g., daily fluxes or spectra over a wide energy range for a complete 11 yr solar cycle, it will become necessary to adapt an automated statistical tool to scan the full parameter space, investigating, e.g., if the rigidity dependence of all three diffusion coefficients is exactly the same, or if drift effects are changing meaningfully toward solar maximum activity; see, e.g., Martucci et al. (2018) and Aslam et al. (2019). Apart from proton spectra, the AMS-02 helium flux data have become available as well (Aguilar et al. 2018a). They reported that the p to He flux ratio at low rigidity has been decreased unexpectedly after 2015 February. Under such circumstances, it is worthwhile to develop an appropriate model and reproduce the time history of the CR helium flux. We should be able to investigate this feature in detail and hopefully find the basic physical explanation for it.[10]

A similar challenge is the interpretation of the observed electron–positron ratio over the period of solar maximum, including the reversal of the IMF polarity during extreme solar activity, first reported using PAMELA data by Munini et al. (2018) and now for AMS-02 data by Aguilar et al. (2018b).

This work is jointly supported by the National Natural Science Foundation of China (41731067, 41774185, U1738128, and 41531073), the National Basic Research Program (973 program) under grant 2012CB825601, and the Specialized Research Fund for State Key Laboratories. X.L. acknowledges Veronica Bindi as host while visiting her group at the University of Hawaii. M.S.P. acknowledges the financial support of the South African National Research Foundation (NRF) under the Competitive Funding for Rated Researchers, grant 98947. M.Z. was supported in part by NASA grants NNX14AJ53G and NNX15AN72G. This material is based upon work supported by the US National Science Foundation under grant No. CNS 09-23050. We thank the anonymous referee for valuable comments.

## ORCID iDs

Xi Luo https://orcid.org/0000-0002-4508-6042
Marius S. Potgieter https://orcid.org/0000-0003-0793-7333
Ming Zhang https://orcid.org/0000-0003-3529-8743
Xueshang Feng https://orcid.org/0000-0001-8605-2159

[10] While our paper was under review, we noted that such a study was performed by Tomassetti et al. (2018) and Corti et al. (2019) with interesting differences.

## References

Adriani, O., Barbarino, G. C., Bazilevskaya, G. A., et al. 2013, ApJ, 765, 91
Aguilar, M., Cavasonza, L. A., Alpat, B., et al. 2018a, PhRvL, 121, 051101
Aguilar, M., Cavasonza, L. A., Alpat, B., et al. 2018b, PhRvL, 121, 051102
Aslam, O. P. M., Bisschoff, D., Potgieter, M. S., et al. 2019, ApJ, 873, 70
Bieber, J. W., Matthaeus, W. H., Simith, C. W., et al. 1994, ApJ, 420, 294
Bindi, V., Corti, C., Consolandi, C., Hoffman, J., & Whitman, K. 2017, AdSpR, 60, 865
Bisschoff, D., & Potgieter, M. S. 2016, ASS, 361, 48
Bobik, P., Boschini, M. J., Della Torre, S., et al. 2016, JGRA, 121, 3920
Boezio, M., Munini, R., Adriani, O., et al. 2017, Proc. ICRC (Busan), 301, 1091
Burger, R. A., & Potgieter, M. S. 1989, ApJ, 339, 501
Burlaga, L. F., McDonald, F. B., Goldstein, M. L., & Lazarus, A. J. 1985, JGR, 90, A12
Burlaga, L. F., McDonald, F. B., Ness, N. F., et al. 1984, JGR, 89, A8
Burlaga, L. F., Ness, N. F., McDonald, F. B., Richardson, J. D., & Wang, C. 2003, ApJ, 582, 540
Burlaga, L. F., Perko, J., & Pirraglia, J. 1993, ApJ, 407, 347
Burlaga, L. F., Schwenn, R., & Rosenbauer, H. 1983, GeoRL, 10, 5
Chhiber, R., Subedi, P., Usmanov, A. V., et al. 2017, ApJ, 230, 21
Chih, P. P., & Lee, M. A. 1986, JGR, 91, 2903
Corti, C., Bindi, V., Consolandi, C., & Whitman, K. 2016, ApJ, 829, 8
Corti, C., Potgieter, M. S., & Bindi, V. 2019, ApJ, 871, 2
Cummings, A. C., Stone, E. C., Heikkila, B. C., et al. 2016, ApJ, 831, 18
Di Felice, V., Munini, R., Vos, E. E., & Potgieter, M. S. 2017, ApJ, 834, 89
Forman, M. A., Jokipii, J. R., & Owens, A. J. 1974, ApJ, 192, 535
Guo, X., & Florinski, V. 2014, ApJ, 793, 18
Heber, B., & Potgieter, M. S. 2006, SSRv, 127, 117
Herbst, K., Muscheler, R., & Heber, B. 2017, JGR, 122, 23
Jokipii, J. R. 1966, ApJ, 146, 480
Jokipii, J. R., Levy, E. H., & Hubbard, W. B. 1977, ApJ, 213, 861
Jokipii, J. R., & Thomas, B. 1981, ApJ, 243, 1115
Kopp, A., Büsching, I., Strauss, R. D., & Potgieter, M. S. 2012, CoPhC, 183, 530
Kóta, J., & Jokipii, J. R. 1983, ApJ, 265, 573
le Roux, J. A., & Potgieter, M. S. 1991, A&A, 243, 531
le Roux, J. A., & Potgieter, M. S. 1992, ApJ, 390, 661
le Roux, J. A., & Potgieter, M. S. 1995, ApJ, 442, 847
Liu, Y. D., Luhmann, J. G., Lugaz, N., et al. 2013, ApJ, 769, 45
Liu, Y. D., Richardson, J. D., Wang, C., & Luhmann, J. G. 2014, ApJL, 788, L28
Luo, X., Potgieter, M. S., Zhang, M., et al. 2016, ApJ, 826, 182
Luo, X., Potgieter, M. S., Zhang, M., & Feng, X. S. 2017, ApJ, 839, 53
Luo, X., Potgieter, M. S., Zhang, M., & Feng, X. S. 2018, ApJ, 860, 160

Luo, X., Zhang, M., Potgieter, M. S., Feng, X. S., & Pogorelov, N. V. 2015, ApJ, 808, 82
Luo, X., Zhang, M., Rassoul, K. H., & Pogorelov, N. V. 2011, ApJ, 730, 13
Luo, X., Zhang, M., Rassoul, K. H., Pogorelov, N. V., & Heerikhuisen, J. 2013, ApJ, 764, 85
Martucci, M., Munini, R., Boezio, M., et al. 2018, ApJL, 854, L2
McDonald, F. B., Lal, Nand, & McGuire, R. E. 1993, JGR, 98, A2
Mewaldt, R. A., Davis, A. J., Lave, K. A., et al. 2010, ApJL, 723, L1
Miyake, S., Kataoka, R., & Sato, T. 2017, SpWea, 15, 589
Munini, R., Boezio, M., Bruno, A., et al. 2018, ApJ, 853, 76
Ngobeni, D. M., & Potgieter, M. S. 2015, AdSpR, 56, 525
Parker, E. N. 1958, ApJ, 128, 664
Parker, E. N. 1965, P&SS, 13, 9
Pei, C., Bieber, J., Burger, R., & Clem, J. 2010, JGR, 115, 12107
Perko, J. S., & Fisk, L. A. 1983, JGR, 88, A11
Potgieter, M. S. 2013, LRSP, 10, 3
Potgieter, M. S. 2014, BrJPh, 44, 581
Potgieter, M. S. 2017, AdSpR, 60, 848
Potgieter, M. S., & le Roux, J. A. 1994, ApJ, 423, 817
Potgieter, M. S., le Roux, J. A., Burlaga, L. F., & McDonald, F. B. 1993, ApJ, 403, 760
Potgieter, M. S., & Moraal, H. 1985, ApJ, 294, 425
Potgieter, M. S., Vos, E. E., Boezio, M., et al. 2014, SoPh, 289, 391
Potgieter, M. S., Vos, E. E., Munini, R., Boezio, M., & di Felice, V. 2015, ApJ, 810, 141
Putze, A., Derome, L., Maurin, D., Perotto, L., & Taillet, R. 2009, A&A, 497, 991
Qin, G., Matthaeus, W. H., & Bieber, J. W. 2002, ApJL, 578, L117
Qin, G., & Shen, Z.-N. 2017, ApJ, 846, 56
Richardson, J. D., Liu, Y., & Wang, C. 2008, AdSpR, 41, 237
Schwadron, N. A., Cooper, J. F., Desai, M., et al. 2017, SSRv, 212, 1069
Stone, E. C., Cummings, A. C., McDonald, F. B., et al. 2013, Sci, 341, 150
Teufel, A., & Schlickeiser, R. 2002, A&A, 393, 703
Tomassetti, N., Barão, F., Bertucci, B., et al. 2018, PhRvL, 121, 25
Vos, E. E., & Potgieter, M. S. 2016, SoPh, 291, 2181
Webber, W. R., & McDonald, F. B. 2015, GeoRL, 40, 1665
Wibberenz, G., Le Roux, J. A., Potgieter, M. S., & Bieber, J. W. 1998, SSRv, 83, 309
Zank, G. P., Adhikari, L., Hunana, P., et al. 2017, ApJ, 835, 147
Zank, G. P., Adhikari, L., Zhao, L.-L., et al. 2018, ApJ, 869, 23
Zank, G. P., Matthaeus, W. H., Bieber, J. W., & Moraal, H. 1998, JGR, 103, 2085
Zhang, M. 1999, ApJ, 513, 409
Zhang, M., Luo, X., & Pogorelov, N. V. 2015, PhPl, 22, 091501
Zhao, L.-L., Adhikari, L., Zank, G. P., Hu, Q., & Feng, X. S. 2017, ApJ, 849, 88
Zhao, L.-L., Adhikari, L., Zank, G. P., Hu, Q., & Feng, X. S. 2018, ApJ, 856, 94
Zhao, L.-L., Qin, G., Zhang, M., & Heber, B. 2014, JGR, 119, 1493
Zhao, L.-L., & Zhang, H. 2016, ApJ, 827, 13